Phenothiazine-Modified PTAA Hole Transporting Materials for Flexible Perovskite Solar Cells: A Trade-Off Between Performance and Sustainability

Daniel Augusto Machado de Alencar, Giulio Koch, Francesca De Rossi, Amanda Generosi, Giuseppe Ferraro, Matteo Bonomo,* Samyuktha Noola, Giulia Pellis, Pierluigi Quagliotto, Barbara Paci, Francesca Brunetti,* and Claudia Barolo

Hole Transport Materials (HTMs) are one of the key elements in Perovskite Solar Cells (PSCs) and specifically polymeric HTMs have recently emerged as one of the most viable options to couple excellent performance and good stability. However, most are processed only in aromatic solvents (e.g., toluene or chlorobenzene), thus negatively impacting the overall sustainability of the device. In this contribution, four novel polymers are synthesized specifically designed to be processable in less harsh, non-aromatic, and non-chlorinated solvent (i.e., Tetrahydrofuran – THF): the conventional PTAA scaffold is modified by the insertion of a phenothiazine (PTZ) and by the modulation of the methyl moieties on the peripheral benzene. Alternatively, a benzothiadiazole moiety is also added. The polymers are then implemented in flexible PSCs (F-PSCs) that have recently attracted increased attention due to their high power-to-weight ratio. The THF-processed P1 (a PTZ-PTAA copolymer with one methyl group substituted) reaches an overall efficiency of 9.10%, outperforming THF-processed PTAA (PCE = 8.25%) and approaching the one of toluene-processed reference (PCE = 9.30%). Furthermore, P1 shows better stability under light soaking conditions. To rationalize these results, different characterizations are presented, including optoelectronic techniques, thermal and surface analyses, and GWAXS measurements.

1. Introduction

Perovskite Solar Cells (PSCs) revolutionized the field of emerging photovoltaic (PV) technology due to their attractive optoelectronic properties and low-cost fabrication techniques.[1] In the last decade, research on PSCs has experienced an exponential rise due to their strong potential to offer a cost-effective and scalable solution for the transition to clean energy production, especially considering their prospective application in tandem configurations for very high efficiency generation.[2] As a result of these, the PSC field has been able to develop power conversion efficiencies (PCE) of up to 26.1% certified with 95% PCE retention after 1200 h (1 Sun, 65 °C).[3]

Recently, flexible Perovskite Solar Cells (F-PSCs) have been emerging as a growing niche aimed at extending the range of applications toward Building Integrated Photovoltaics (BIPV), Internet of

D. A. M. de Alencar, G. Ferraro, M. Bonomo, S. Noola, G. Pellis, P. Quagliotto, C. Barolo
Department of Chemistry, NIS and INSTM Reference Centre
Università degli Studi di Torino
Via Pietro Giuria 7, Torino 10125, Italy
E-mail: matteo.bonomo@unito.it

G. Koch, F. De Rossi, F. Brunetti
CHOSE – Centre for Hybrid and Organic Solar Energy, Department of Electronic Engineering
University of Rome ''Tor Vergata''
Via del Politecnico 1, Rome 00133, Italy
E-mail: francesca.brunetti@uniroma2.it

A. Generosi, B. Paci
SpecX-Lab
Istituto di Struttura della Materia CNR
Via del Fosso del Cavaliere 100, Roma 00133, Italy

C. Barolo
ICxT Interdepartmental Centre
University of Turin
Lungo Dora Siena 100, Torino 10153, Italy

C. Barolo
Istituto di Scienza
Tecnologia e Sostenibilità per lo sviluppo dei Materiali Ceramici (ISSMC-CNR)
Via Granarolo 64, Faenza, RA 48018, Italy

Things (IoT), portable electronics, and even space applications.[4] The appeal of these devices is ascribable to their projected high power-to-weight (PWR) and scalable roll-to-roll (R2R) processing using lightweight and bendable substrates,[4] proving a more economical alternative to the rigid-glass based devices. The efficiency of F-PSCs has accompanied the rapid development experienced by conventional glass substrate devices, rising from 2.62%[5] in 2013 to the record 25.09%[6] (certified 24.9%) in 2024 (n-i-p architecture). However, to unlock F-PSCs full commercialization potential, research must focus efforts in boosting the performance, stability, and sustainability of the devices;[7] in this context, the development of device charge transport layers, namely Hole- and Electron Transport layer (HTM and ETM, respectively) will be essential.

In n-i-p architectures, HTMs are deposited on top of the active layer and play a fundamental role in extracting generated p-type charge carriers from the perovskite (PSK) layer and delivering them to the counter electrode. In fact, the ideal HTM must generally have (i) comparable energy levels to the valence band of the perovskite photoactive layer, (ii) high hole mobilities, (iii) thermal and photostability, and (iv) a scalable, low-cost synthesis, avoiding harsh chemicals and processes.[8] A wide range of organic and inorganic materials have extensively been studied for their applications as HTMs in PSC's. Most famous inorganic examples[9] employ NiO_x,[10] $CuSCN$,[11] MoO_x,[12] While these materials reveal appropriate optical and electronic properties, and are sustainable from the point of view of synthesis cost and element abundancy, they are still very restricted and limited to p-i-n architectures.[13] This is because: (i) requirement of high temperature annealing processes to perform smooth and defect-less thin films, and (ii) poor solubility in a restricted window of polar solvents, making them incompatible with n-i-p architectures, where the HTM is deposited on top of the perovskite layer.[13] Therefore, and specifically in the context of F-PSCs, organic HTMs have proven to be more promising compared to their inorganic counterparts, in part due to easier synthetic modification allowing for the fine tuning of optical, electronic, and structural properties to different perovskite requirements and, most importantly, milder (considerably lower temperature) depositions, which are also less energy-demanding from a sustainable point of view, and wide solubility in most processable solvents.[14]
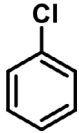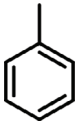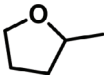
For both rigid and F-PSCs, polymeric organic HTMs can solve the main instability issues that arise from small molecules HTMs (e.g. spiro-OMeTAD[15]), as the former presents improved film-ability, improved charge transfer properties, and a more effective hydrophobic barrier.[8] Among others (e.g., P3HT,[16] PEDOT:PSS[17]) Poly(triarylamine) (PTAA), is one of the most common polymeric HTM in n-i-p architectures, reaching an impressive PCE as high as 22.1%[18] (small area rigid, n-i-p, employing PTAA as HTM) since its first introduction in 2013.[19] Its widespread use is justified by remarkable thermal stability (related to its amorphous state), relatively good hole mobility even in its pristine form (i.e., without dopants), and suitable band alignment with panchromatic perovskite absorbers.[20] To achieve high efficiencies, PTAA is still commonly processed in toxic, aromatic, and halogenated solvents such as chlorobenzene (CB) or toluene,[21] that are extremely hazardous to marine aquatic life according to their hazard statements. That is particularly critical if the deposition method of the HTMs is based on solvent-

wasting approaches as is spin-coating. Moreover, this also represents a criticality toward the scalability of the approach, as during the annealing step, the direct emission of harsh organic solvents and their thermally-generated byproducts into the atmosphere contributes to air quality deterioration. Quite dramatically, the use of chlorobenzene as solvent in HTM deposition contributes to nearly up to 10% of overall impact of PSCs in terms of human toxicity.[22] Last but not least, the substitution of unhealthy human and environmentally damaging solvents with the green counter parts should be a pillar as the projected industrialization of F-PSC's should be based on open air production process. Indeed, paving the way for industrialization of sustainable F-PSCs will enable the exploitation of alternative production process such as roll-to-roll, which is well established in the organic photovoltaics (OPV) field,[23] toward unconventional exploitation of solar cells, e.g. agrivoltaics[24] and building integrated photovoltaic (BIPV).[25] Unfortunately, these solvents are commonly employed out of necessity for high efficiency, due to the restricted solubility that results from the strategic design for high-performing polymeric HTMs (PTAA) where an extended π-π conjugation framework and a high molecular weight is preferred.[26] This issue cannot be ignored toward the scalability, and the eventual commercialization and market acceptability of PTAA-based PSCs. The search for green-harmless solvents to process HTMs should be at the forefront to ensure the safe and sustainable upscale of PSCs.[27]

Although some groups in literature have attempted to tackle this issue, the use of green solvents to deposit hole transport layers is still largely unnoticed in literature. Lee et al.[28] developed a novel polymeric HTM that exhibits high solubility in non-aromatic solvents like 3-methylcyclohexanone (3-MC), reporting competitive PCE values (19.9%, n-i-p, rigid). Indeed, 3-MC can be found naturally occurring in peppermint oil[29] and is an approved food flavoring agent by the European Food Safety Authority;[30] however, despite its natural availability and low toxicity, 3-MC is still too expensive (600€ L^{-1} from Sigma-Aldrich) to pursue the low-cost commercialization of PSC. Conversely, an attractive candidate showing a promising trade-off between environmental and health friendliness versus price is tetrahydrofuran (THF). THF (70€ L^{-1} from Sigma-Aldrich) is a non-aromatic, non-chlorinated, low environmentally risk solvent and shows a low human health toxicity when used in PSCs processing;[31] even more interestingly, these features are coupled to the possibility of exploitation of some greener and bio-renewable structural analogues, such as 2-MeTHF, that can be directly derived from furfural **Table 1**.[32] In the PSCs' field, THF has already been proposed as a greener alternative to chlorobenzene when depositing spiro-, managing to achieve record efficiencies of 17%. (n-i-p, rigid, undoped spiro-)[33] Lu et al.[31b] also proposed THF as a greener solvent (reference = CB) to process a novel carbazole-based dopant-free small molecule HTM (3 mg/ml), displaying better film-ability and achieving a PCE of 17.2% (rigid, n-i-p). Additionally, the choice of green solvent processable HTMs is a more critical parameter for polymers when compared to small molecules due to their limited solubility, making these results very promising toward the sustainable upscaling of F-PSCs.

Aiming at designing a THF-soluble polymeric HTM, in this paper, the PTAA main backbone[34] is modified with phenothiazine (PTZ)-based or benzothiadiazole (BTD) based units. PTZ

**ADVANCED
SCIENCE NEWS**

www.advancedsciencenews.com

**ADVANCED
SUSTAINABLE
SYSTEMS**

www.advsustainsys.com

Table 1. Table exploring environmental hazards and prices of different solvents proposed for hole transporting layers processing.

Solvent	Chlorobenzene	Toluene	Tetrahydrofuran	2-Methyltetrahydrofuran
Environmental Hazards [a]	H411	H412	–	–

[a] Data extracted from SDS Charts.

is a promising scaffold to tackle the upscaling of F-PSCs due to its good solubility in common organic solvents, its high chemical stability, easy tunability of its functionalization, high hole mobilities, and its low cost ($0.089€$ g^{-1} from Sigma-Aldrich); indeed, it has been already exploited as the main building block for HTMs toward efficient PSCs.[35] Benzothiadiazole (BDT) is also widely reported among organic HTMs in literature due to its donor-acceptor (D-A) character, tuneable nature, and electron-deficient system, giving rise to an easy tunability of the electronic properties.[36] Herein, we report four novel THF-soluble polymeric scaffolds that are primarily based on phenothiazine with differently substituted triphenylamine (TPA) units and benzothiadiazole scaffolds. To the best of our knowledge, the coupling of these units has only been limited to small molecules in literature without being yet extended to polymeric systems. Aiming at a fair internal comparison, we used PTAA as a reference. We decided to initially apply and optimize the polymeric HTMs on n-i-p flex devices. However, although PTAA is conventionally employed as HTM in p-i-n flexible devices,[37] as far as we are aware, there are no examples of n-i-p flexible PSCs devices employing PTAA as the HTM; as such, this work would provide one of the first literature references. As the main result, some of the specifically designed HTMs achieve comparable efficiencies to PTAA processed with toluene and even outperform PTAA processed with THF.

2. Results and Discussion

2.1. Material Synthesis and Characterization

Throughout this paper, the attention is focused on the improvement of the greenness of the HTM, both in its synthesis and deposition. Aiming at this, we faced the thoughtful design of novel HTMs' synthetic pathway toward the greenest possible one. The synthetic design was initiated by the preparation of the modified-brominated-triphenylamine monomers **1,2**, and **4**. (**Scheme** 1A) whereas for monomer **3**, no synthetic protocol is presented as the molecule is available commercially.

A Buchwald-Hartwig amination enabled the formation of a carbon-nitrogen bond to produce the modified triphenylamine scaffolds with their respective methyl substitutions (i and ii). This was achieved with very high yields ($\approx 90\%$) and moderate reaction times (≈ 4 h) that afforded straightforward purification procedures. The selective brominations of i and ii were achieved using N-bromosuccinimide (NBS) in mild conditions, obtaining at moderate to high yields ($50 - 90\%$), the brominated monomers **1** and **2**. A different approach was taken to prepare monomer

4. Instead, a Suzuki-Miyaura protocol, which already complies with most of the Green Chemistry principles,[38] due to its high yield, mild reaction conditions, and wide availability of inert, stable, and low-toxicity organoboron reagents, was applied by the coupling of commercially available dibrominated benzothiadiazole and triphenylamine boronic acid units, moderately yielding **iii**. ($\approx 50\%$) The final step involved applying the bromination protocol as used for **1** and **2**, yielding **4**. ($\approx 90\%$ yield) Due to its attractive sustainable characteristics mentioned previously, the Suzuki-Miyaura Polycondensation (SMP) reaction was chosen for the production of **P1-P4**. (See Figures S1-S10, Supporting Information).

In this view, the choice of PTZ as a scaffold is strategic, considering its remarkable versatility and easiness of functionalization. PTZ was initially modified by introducing an alkyl hexyl chain at the N-position to ensure high solubility and good processability in common organic solvents, primarily when the monomer would be implemented in a polymeric chain. 10-hexyl-3,7-bis(4,4,5,5-tetramethyl-1,3,2-dioxaborolan-2-yl)-10H-phenothiazine was thus obtained using established protocols developed by our research group[39] and was used as a common monomer for all novel polymers **P1-4**. After Soxhlet extraction, the purified polymers were reported with moderate to high yields. ($\approx 50 - 80\%$) (Scheme 1B) An estimation of the synthetic price of **P1-4** was conducted, proving the low-cost feature of our materials. (See Figures S11–S20, Supporting Information) Overall, we estimated the following costs: **P1**: 41.09 € g^{-1}, **P2**: 52.73 € g^{-1}, **P3**: 100.62 € g^{-1}, and **P4**: 56.00 € g^{-1}, which are almost two orders of magnitude cheaper than the prices of commercial **PTAA** (e.g., ≈ 3 K€ g^{-1} from Sigma-Aldrich, when the Mw is comparable with the **P1-4** ones), paving the way for industrial exploitation of **P1-4** in F-PSC. One should note that **P3** doubles the price of **P1**, **P2**, and **P4**, solely because of the use of the commercial monomer **3** and its higher price.

The four novel polymers were then thoroughly characterized for their structural, optoelectronic, and thermal properties **Table** 2. Only ^1H NMR spectroscopy was used to confirm the chemical structures of polymers **P1-4**, as the resolution in ^{13}C NMR was too poor for any signal assignment. (See Figures S7–S10, Supporting Information). The prominent peaks are located in the aromatic region at ≈ 7 ppm, which can be attributed to de-shielded protons from the PTZ benzene rings, as well as those belonging to the TPA and the BDT; these peaks resound at slightly different chemical shifts compared to the starting monomers, evidencing the completion of the coupling reaction. Furthermore, in the aliphatic region of the spectrum, one can
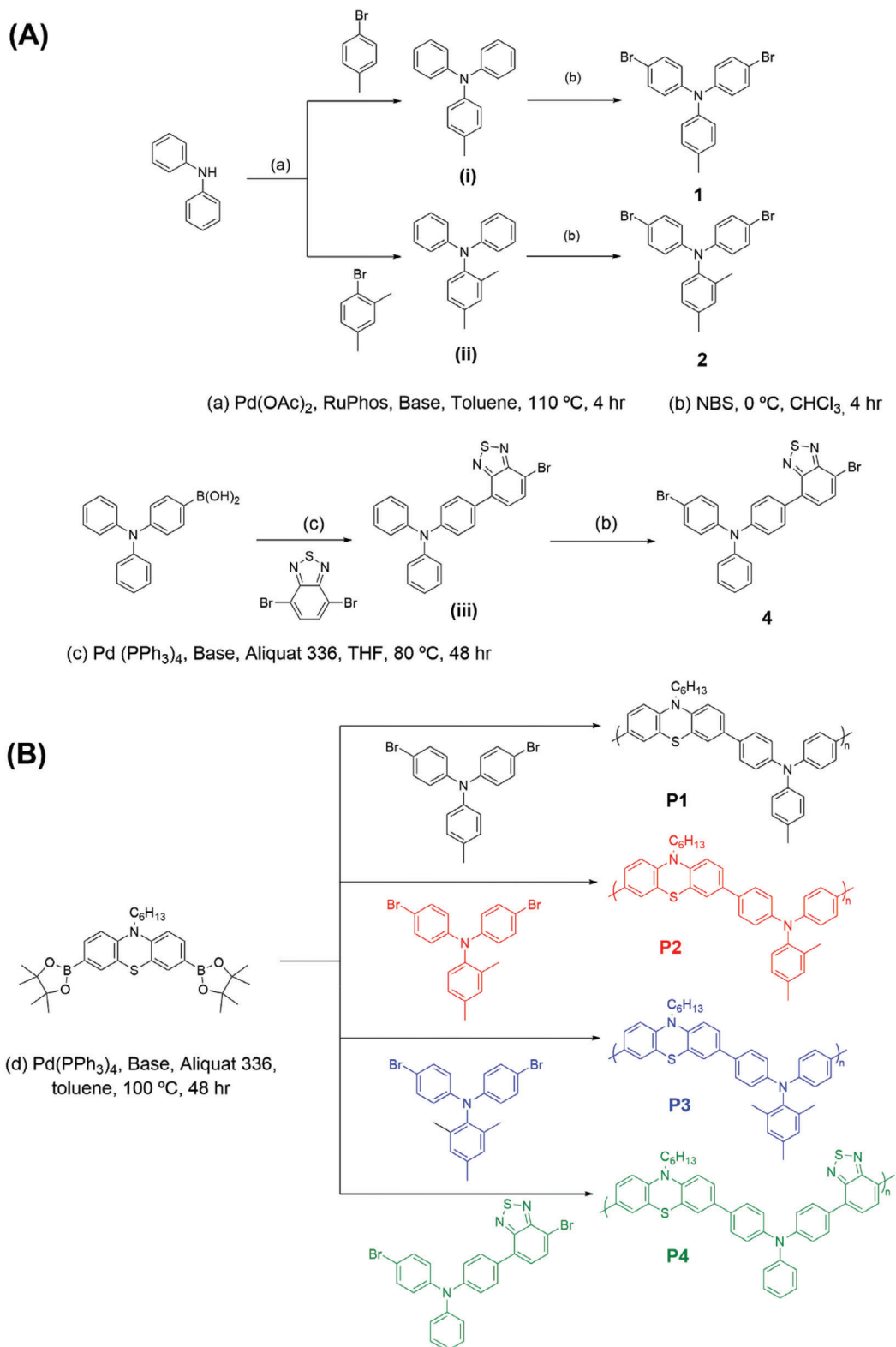
**ADVANCED
SCIENCE NEWS**

www.advancedsciencenews.com

**ADVANCED
SUSTAINABLE
SYSTEMS**

www.advsustainsys.com

Scheme 1. Synthetic strategy for: A) Monomer's **1, 2, and 4** B) Polymers **P1-4**.

**ADVANCED
SCIENCE NEWS**

www.advancedsciencenews.com

**ADVANCED
SUSTAINABLE
SYSTEMS**

www.advsustainsys.com

Table 2. Summary of optoelectronic Parameters of **P1-4** and **PTAA**.

Polymer	E_{HOMO} [eV]	E_g [eV]	E_{LUMO} [eV]	λ_{abs} sol. [nm]	λ_{emi} [nm]	λ_{abs} film[nm]
P1	−5.21	2.92	−2.29	360	475	358 [a]
P2	−5.33	2.96	−2.37	360	475	367 [a]
P3	−5.17	2.96	−2.21	365	472	374 [a]
P4	−5.14	2.25	−2.89	470	740	510 [a]
PTAA	−5.14	2.96	−2.18	386	378	411[b]

[a] (Film deposited with THF);   [b] (Film deposited with toluene).

also identify peaks related to the hexyl alkyl chain present on all PTZ scaffolds and the ones of the methyl groups (in ortho, meta, and para position) of the triarylamine unit. The increased broadness of proton peaks of the products spectra compared to the monomers ones is a typical feature in the NMR of polymeric compounds due to increased electron delocalization following on from the increase in both Molecular weight (M_W) and viscosity.[40]

Gel Permeation Chromatography (GPC) was used to measure the molecular weights (M_w) and polydispersity index (PDI) of polymers **P1-4** (See Figure S21, Supporting Information). The SMP protocol for polymers **P1-4** produced systems of similar molecular weights in the range of 10–20 kDa. Furthermore, the low polydispersity index means that all chains are very similar in length, which in turn can result in improved structural and electronic properties. Such M_w values, although moderately low, agree with the literature ones obtained by SMP protocols.[38]

UV-visible spectra display a high energy band at 320–380 nm, typical for **P1-4**, which can be attributed to the π-π* transition of the polymer backbone conjugation from the aromatic rings belonging to the PTZ and the TPA units.[41] Indeed, this can be confirmed by the bathochromic shift observed with respect to the absorption profiles of the monomers used caused by the extended delocalization of π electrons[42] (See Figure S22, Supporting Information). While UV-visible spectra present a single sharp absorption band at 320 nm for **P4**, **P1-3** show a considerably broader absorption range, characterized by the presence of a shoulder, blue-shifted with respect to the main peak, ascribable to the absorption of TPA moiety.[41a] Moreover, the main peaks in **P1-3** are blue-shifted with respect to **PTAA**, most likely due to the electron-rich phenothiazine acting as an electron donor, leading to a slightly wider band gap of the systems.[43] **P4** displays a second peak, red-shifted of ≈100 nm, likely due to the absorption of the BDT unit. Indeed, this absorption peak arises from the charge transfer dynamics of the polymeric chain as a result of the donor-acceptor character of the final copolymer.[44]

The intensity of the most hypochromic peaks at ≈330 nm changes as a function of the methyl substitution. Indeed, these features could be ascribable to an inter-chain charge transfer caused by the inherent π stacking of systems with similar twisted polymeric planes.[45] Indeed, the stacking is made more complicated by the increased substitution of the methyl groups, which distorts the torsion of the polymer backbone,[46] thus reducing the intensity of the signal. The inter-chain charge transfer is also noted for **PTAA** but at a significantly lower intensity with respect to **P1-3**. Indeed, the phenothiazine scaffold could act as a π-bridge, heavily influencing the conformational configuration

of the polymer backbone and thus facilitating the long-range order.[47]

UV/Vis absorption and emission spectra (**Figure 1a,b**) allow a fair estimation of the optical band gap (E_g) of the systems. The estimation of the E_g was obtained by dividing 1240 by the wavelength of the normalized onset absorption.[48] **P1**, **P2**, and **P3** display a negligible change on the E_g. Indeed, it seems that the inductive effect of the electronic donating methyl groups is "quenched", most likely due to the nitrogen atom present at the TPA, breaking the π-π conjugation of the polymeric system. **P4** experiences a significant lowering of the E_g of around 0.60 eV due to the electronic withdrawing behavior of BDT,[36] which directly conjugates with part of the system.[43]

Cyclic Voltammetry (CV) was performed to estimate the energy of the Highest Occupied Molecular Orbital (HOMO). Indeed, the HOMO can be estimated by measuring the oxidation potential versus Fc/Fc$^+$ as internal reference, and then by referring it to vacuum (E (versus vacuum) = -(5.1 + E_{ox}(V versus Fc/Fc$^+$)). **P1**, **P3**, and **P4** revealed very favorable HOMO energy levels (-5.21 eV, -5.17 eV, and -5.14 eV, respectively, comparable to PTAA's one, located at -5.14 eV versus vacuum) to allow the hole extraction from the perovskite's valence band (Figure 1d). Indeed, the latter is located high enough in energy to assure a quantitative hole extraction while minimizing the probability of recombination events.[49] On the other hand, **P2** exhibits a deeper HOMO that is energetically closer to the valence band of the perovskite, leading to a more probable competition between hole extraction and electron injection, negatively impacting the efficiency of the device. Unfortunately, the LUMO energy level was experimentally inaccessible by CV (i.e., no peak could be seen in the reduction scan). Therefore, to estimate the LUMO energy level of our novel HTMs, we could combine the HOMO energy level and optical band gap previously estimated by applying this equation: LUMO (eV) = HOMO (eV) – BG (eV).[50] The LUMO level of **P1-4** was found to be higher than the perovskites conduction band, which provides an additional thermodynamic barrier for any back-electron injection occurring into the HTM, which would cause recombination events with the generated holes, resulting in poorer efficiencies.

To examine the operational window of the novel HTMs, the thermal stability of polymer **P1-4** is assessed using Thermogravimetric Analysis (TGA). T_{stab} was established as the temperature at which a 5% weight loss is observed. TGA thermograms (**Figure 2a**) all displayed T_{stab} above 350 °C, showing no release of solvent or water (even at lower T), further reinforcing the purity degree ensured by the synthetic protocols. More importantly, our novel HTMs would not degrade at operational temperatures
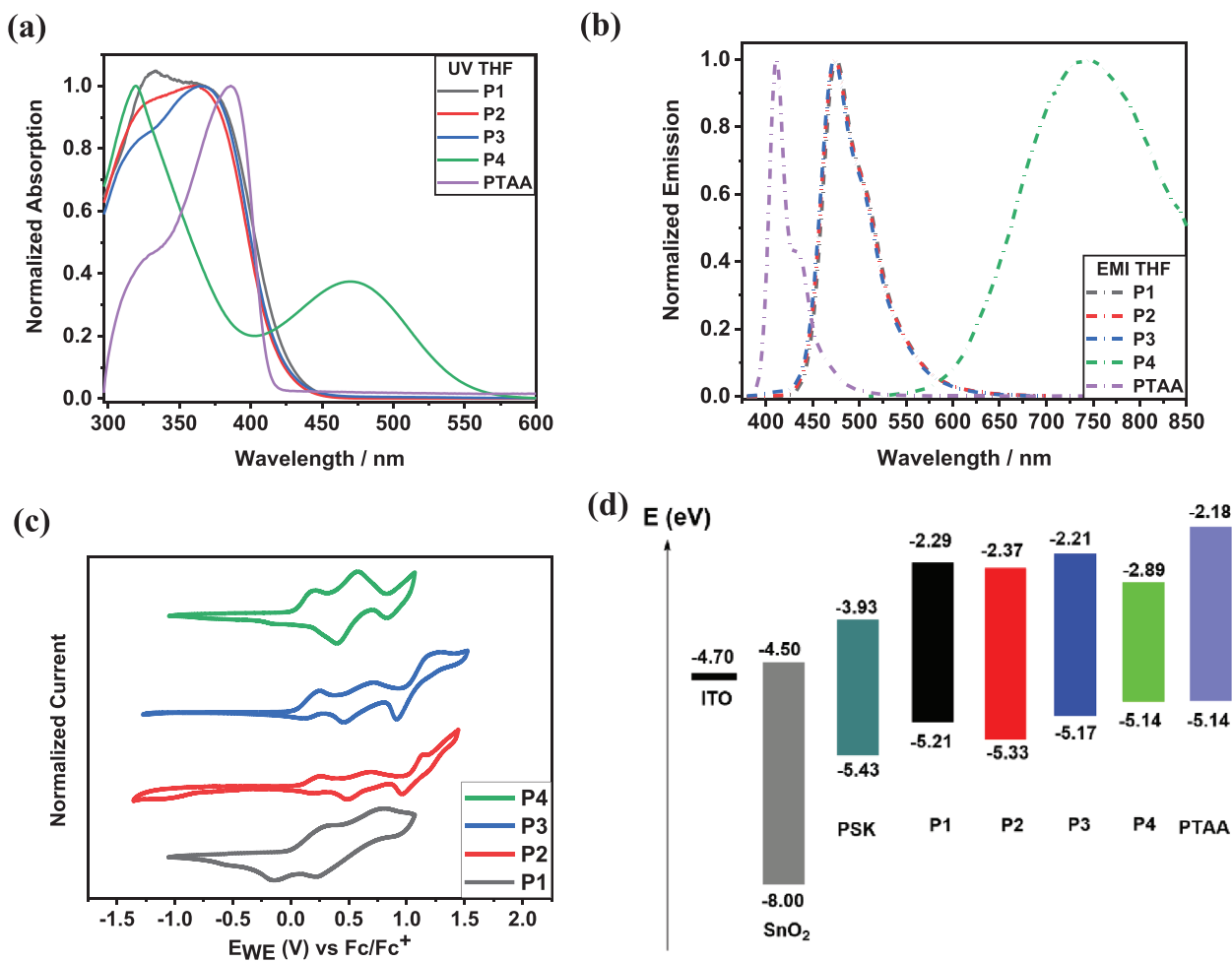
Figure 1. a) UV spectra in solution **P1-4** and **PTAA** (3.0×10^{-2} mg mL^{-1} in **THF**) b) Fluorescence spectra in solution (THF) **P1-4** and **PTAA** (3.0×10^{-2} mg mL^{-1} in **THF**) c) Cyclic Voltammograms of **P1-4** in DCM d) Summary of Energy levels of **P1-4**.

that devices would experience (< 80 °C).[51] Aiming for the production of a stable HTM, any conformational modification of the polymer within the operational temperature should be avoided, besides degradations; indeed, any heat-induced change could alter the interfacial dynamics between HTM/perovskite or HTM/electrode, creating possible defects and recombination sites. To monitor the conformational transition of the polymeric chains, Differential Scanning Calorimetry (DSC) was exploited. From the DSC thermograms (Figure 2b), **P1-3** revealed an indicative glass transition temperature (T$_g$) ranging from 195 °C
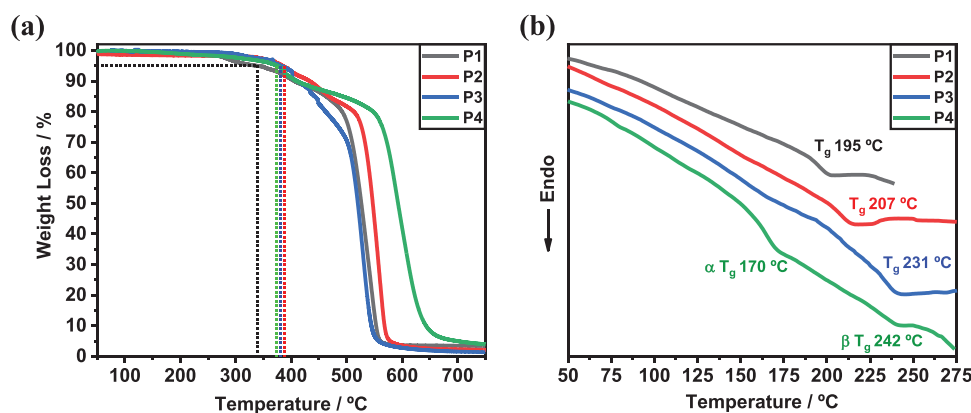

Figure 2. a) TGA of HTM's **P1-4** in Air b) DSC of HTM's **P1-4** in N$_2$.

**ADVANCED
SCIENCE NEWS**

www.advancedsciencenews.com

**ADVANCED
SUSTAINABLE
SYSTEMS**

www.advsustainsys.com

(**P1**) to 231 °C (**P3**), indicating a marked amorphous nature of the polymers. The peak is slightly shifted to higher temperatures as the methyl substitution on the triphenylamine ring increases. This implies that the higher the number of methyl groups is, the better the polymer stability toward heat-induced morphological modification, most likely due to a stiffer polymer backbone that inhibits chain mobility.[52] **P4** shows a double glass transition, with a first one at ≈175 °C and a subsequent one at ≈240 °C. These two glass transitions could be most likely attributed to the random block copolymer chain structure of **P4**. Indeed, due to the synthetic procedure selected, monomer **4** has not a preferential coupling site to the PTZ monomer, leading to a polymeric mixture with different structural domains.[53]

2.2. Device Performance

Nowadays, dopant-free HTMs are preferred in the production of stable devices because they do not suffer from dopant-induced degradation.[54] Furthermore, dopant-free HTMs are also valuable from a sustainable point of view, as often, dopants include elements (e.g., Li, Co) that are characterized as *critical raw materials*.[55] Therefore, it was decided to evaluate if **P1-4** would initially work in their pristine forms (i.e., undoped): indeed, the PTZ has already been mentioned as a promising scaffold for dopant-free application, combining an electron-rich structure with good hole mobility.[56] We selected commercial PTAA for the reference for this study due to the chemical similarity to our polymers. We resorted to *Low Mw – 10 kDa* (**PTAA**$_{LMw}$) as a reference due to the MW similarity to **P1-4**. However, a high MW has been proved to be beneficial for the device performances,[57] therefore, as an additional reference, we also employed *High Mw – 100 kDa* (**PTAA**$_{HMw}$). Besides THF (i.e., the selected solvent for greener processing), **PTAA**$_{LMw}$ performance was also evaluated using toluene to comply with deposition procedures reported in the literature.[21] It is important to recall here that **PTAA**$_{HMw}$ was deposited using Toluene only due to its very poor solubility in THF.

Unfortunately, when implemented as dopant-free HTMs, **P1-4** (≈ 0.5%) are not able to perform efficiently, especially when compared to **PTAA** (≈ 2–4%), the potential of which has already been showcased even in dopant-free fashion.[58] (See Figure **S23**, Supporting Information). Thus, differently from what was expected, the PTZ moiety does not improve the charge carrier transport of the HTM. A possible explanation for the low efficiency of undoped HTMs could be related to the lack of specific palladium-purification procedures from the synthetic protocols used. Indeed, it is well known in literature that Pd-nanoparticles, that can result from residual Pd-based catalysts employed in the synthetic protocols, have a large affinity toward conjugated π systems.[59] These could ultimately play the role of charge trap sites making the unwanted recombination reaction more likely, thus trapping mobile charges and hampering the charge transport properties of the material.[60] We are currently working on this aspect, training to obtain Pd-free HTMs to be further used in PSCs toward further more sustainable devices.

To have a closer look at the un-doped HTM film quality and polymer chain ordering, we initially analyzed the differences between **P1-4** respective solution and solid state, as this can give us a
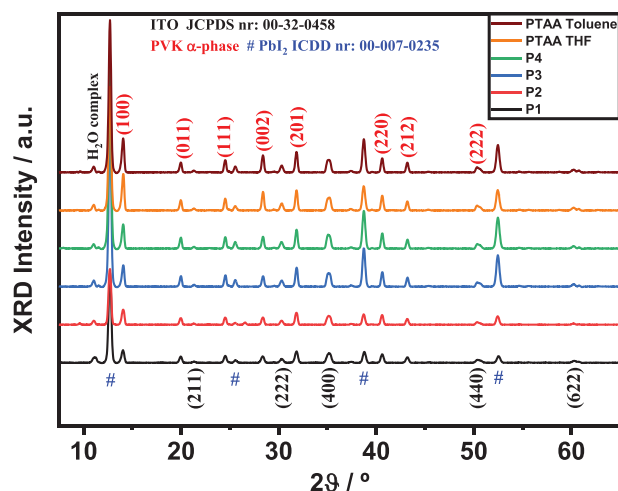

Figure 3. XRD Pattern of **P1-4** and **PTAA**$_{LMW}$ in **THF** and **Toluene**. α-phase triple cation perovskite polycrystalline structure is observed, Miller indexes being reported in red. Monocrystalline PbI$_2$ precursor peaks are represented by blue # label. Monohydrate perovskite complex (CH$_3$NH$_3$*H$_2$O)PbI$_3$ (101) reflection (monoclinic P$_{21}$/m crystal structure) at 10.70° is detected. Almost negligible δ-FAPbI$_3$ signal can be observed at ≈11.20°.[64]

strong indication of the polymer re-arrangement upon undergoing reconfiguration between the two phases.[61] **P1-4** show minimal differences in the absorption maxima of most bathochromic peaks when passing from solution state to solid state (See Figure S24, Supporting Information), indicating that these polymers do not seem to undergo much of a configurational change upon deposition. This could evidence the formation of pre-aggregates in solution that dictate the morphology of the film.[61] This is very beneficial as a high degree of pre-aggregation in solution seems to translate to larger domains that have a higher uniformity over longer ranges of order, thus enhancing charge carrier properties.[62]

We extended our film analysis to include Grazing incidence Wide Angle X-ray Scattering (GWAXS) and X-Ray Diffraction (XRD) measurements. XRD patterns of pristine PSK films were compared with the one of PSK/HTM stacked layers to evidence any crystallographic modification induced by the deposition of **P1-4** and **PTAA**$_{LMW}$ (both in Toluene and THF) on top of the PSK. As reported in **Figure 3**, the [001] orientation is detected, all (and only) reflections starting from (001) up to (004) being labelled accordingly to JCDD card nr: 00-007-0235, Crystal system: Hexagonal, Space group: P-3m1, Space group number: 164, a (Å) = b (Å) = 4,5570, c (Å) = 6.9790.[63] No meaningful differences were found when PSK/HTM layer was analyzed (Figure 3), indicating that the perovskite structure is influenced neither by the HTM layer nor by the solvent used for the deposition. Additionally, spurious reflections ascribable to **P1-4** or **PTAA**$_{LMw}$ are not detected, owing to the amorphous nature of the HTM layer.

GWAXS was then exploited on samples prepared with undoped polymers to gain helpful information on the short-range packaging of polymer chains. All the polymers displayed an "edge on" configuration, evidenced by the presence of the (100) reflection at 2θ ≈ 3°.[65] (**Figure 4**) This implies that the phenothiazine hexyl side-chain and triarylamine methyl substitution
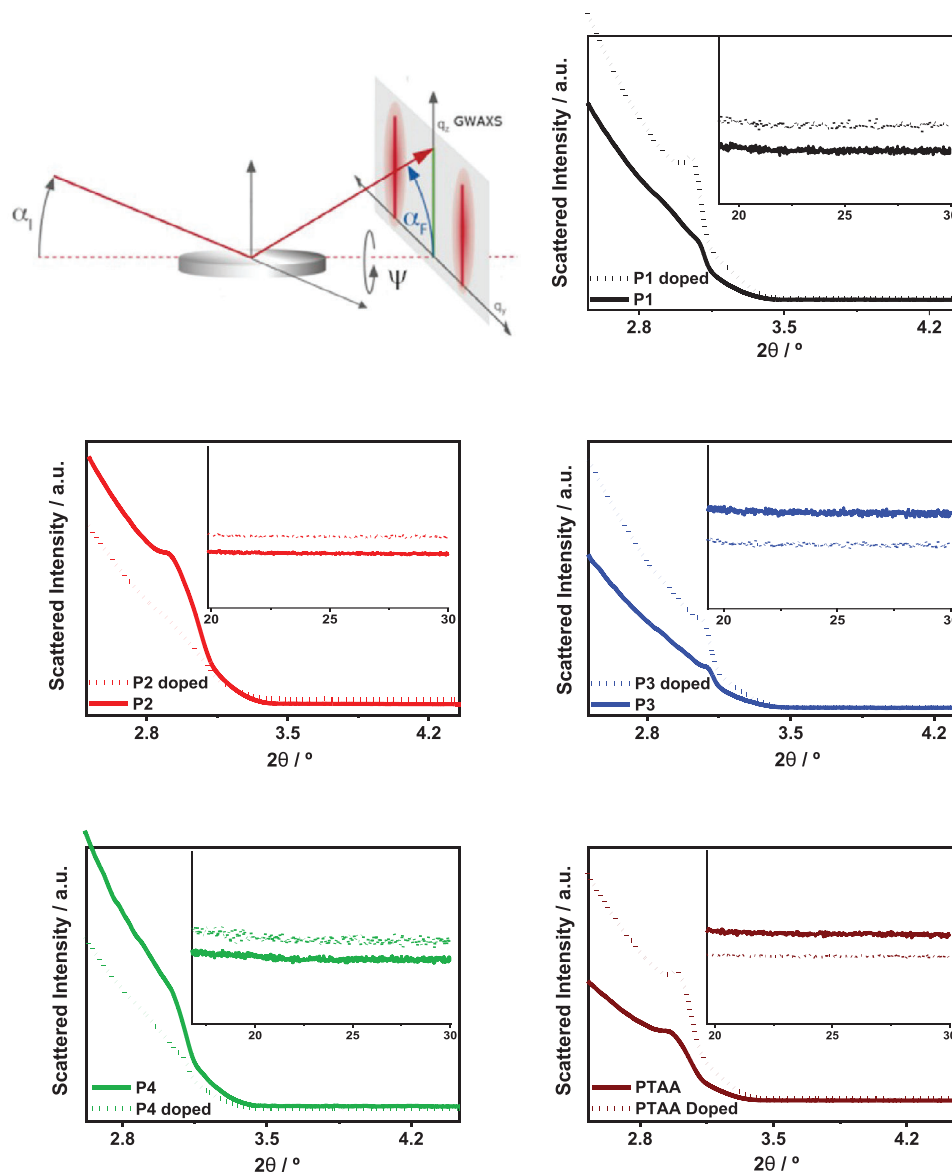
Figure 4. Sketch of the experimental GWAXS setup and GWAXS patterns collected upon the pristine and doped polymers. In the inset of each image, the high angle XRD patterns are reported: the absence of the (010) reflection validates the "edge on" configuration.

heavily influence the way that the polymer, upon transforming to the solid state, anchors to the perovskite and stacks within itself.

GWAXS measurements on the polymeric films could also be used to extract quantitative data regarding the polymeric grain sizes (also defined as Coherent Crystalline Length – CCL)[66] and the polymeric interplanar spacing[66] (**Table 3**). Interestingly, as visible in Figure 4, slight differences in the peak positions for different polymers are found (inversely related to interplanar distances via Bragg's Law). In the undoped state, **P2** was found to have the most significant interplanar spacing (30.2 Å), followed by **PTAA**$_{LMw}$ (29.7 Å) and **P4** (29.1 Å), while **P1** and **P3** show the same d-spacing (28.6 Å). These latter polymers are also those exhibiting the most extensive crystalline domains (highest CCL), with **P1** and **P3** having an average crystallite dimension as high as 75.5 nm (corresponding to 26 repetition units) and 60.7 nm (cor-

responding to 21 repetition units), respectively. From this data, it could be inferred that the unsymmetrical methyl substitution of **P2** creates disorder in the structure and consequently increases the spacing between planes. On the other hand, **P1** has a symmetrical side unit, with a single methyl moiety producing a more flexible backbone and, thus, the narrowest packing and the largest domain sizes.[67] These parameters would result in a lamellar structure more advantageous for hole-charge transfer, whereas large crystalline grains can also help slow down recombination reactions.[57b] The effect of incorporating the phenothiazine unit on interplanar spacing can be clearly observed if **PTAA**$_{LMw}$ and **P3** are compared. **P3** shows smaller (-1Å) interplanar spacing with respect to **PTAA**$_{LMw}$, most likely due to a combination of the increased conjugation induced by the electron-rich PTZ scaffold: indeed, it allows stronger π-π^* interactions between polymer

**ADVANCED
SCIENCE NEWS**

www.advancedsciencenews.com

**ADVANCED
SUSTAINABLE
SYSTEMS**

www.advsustainsys.com

Table 3. Quantitative evaluation of structural parameters as obtained by Gaussian fitting procedure of the edge-on (100) reflection.

Sample	d spacing [Å]	Grain size [nm]	Repetition units
P1	28.7 (1)	75.5 (5)	26
Doped **P1**	28.9 (1)	96.5 (5)	33
P2	30.2 (1)	24.0 (5)	8
Doped **P2**	30.4 (1)	28.2 (5)	6
P3	28.6 (1)	60.7 (5)	21
Doped **P3**	28.7 (1)	63.5 (5)	22
P4	29.1 (1)	20.4 (5)	7
Doped **P4**	28.5 (1)	58.0 (5)	20
PTAA	29.7 (1)	26.8 (5)	9
Doped PTAA	29.6 (1)	46.9 (5)	16

chains as a consequence of an "anchoring effect".[68] Finally, **P4** interlamellar spacing also does not differ by much to **P1** and **P3**. It seems that the extra torsion induced in the polymer backbone derived from having an additional 3rd scaffold present (BTD) does not induce a larger d-spacing, meaning that the vertical charge transport properties would most likely not differ by much.

Due to the failure in obtaining dopant-free devices showing good performance, we resolved to use dopants to increase the charge transport ability of our HTMs. State-of-the-art PTAA is usually doped with lithium bis(trifluoromethanesulfonyl)imide (LiTFSI) and tert-butyl pyridine (tBP) to increase carrier mobility and lifetime.[18,69] The doping mechanism of triphenylamine derivatives has been extensively studied[70] and proceeds via one-electron oxidation, forming a radical cation. Indeed, this radical cation is generally unstable and generally leads to the formation of a dimer structure via an irreversible oxidative coupling of two radical cation molecules. Aiming at reducing the variables in the analyses and a fairer comparison with **PTAA**, we decided to dope our polymers with the dopants listed above at a fixed concentration (See Device Fabrication). It must also be considered that the phenothiazine scaffold present in **P1-4** can also be used as an extra oxidation site as the phenothiazine is also good at creating stable 1-cationic radical species.[71]

Before implementing the doped HTMs in complete devices, we investigate the effects of doping on the polymeric film properties by GWAXS. It was found that **P1** was the sample undergoing the most significant crystallinity degree enhancement ($\approx$ +300%), also experiencing an enlargement of CCL (+27%), increasing from 26 to 33 repetition units per crystallite, being the largest amongst all samples. **PTAA**$_{LMw}$ experiments less dramatic increase in both grain size and CCL. Differently, **P2** was found to be the only polymer shortening its CCL after doping (-25%), the doping reducing the short-term order of the polymeric crystallites, whereas **P3** morphology was found to be relatively insensitive to doping in terms of both interplanar distance and CCL, although a crystallinity enhancement was noticed. A peculiar behavior is observed for **P4**, for which the interplanar distance is reduced upon doping, causing a closer packing of the polymeric chains.

The effect of the doping on the HTM film is clearly visible even when UV-Vis spectra of doped and undoped films (See Figure S25, Supporting Information) are compared. For **P1**, we observe

a broad red-shifted absorbance peak emerging in the doped state; this most likely indicates an additional electronic transfer caused by the oxidation of the TPA and PTZ into their cationic-radical state.[72] Moreover, it has been reported that the radical cation is stabilized when electron donating groups (i.e., methyl) are substituted in the *para* position, explaining the high intensity of the additional peak.[73] A similar behavior is observed for **PTAA**$_{LMw}$, whose increment in grain size and CCL (+78%) is coupled with the rise of a low-intensity broad peak at $\approx$ 500 nm, proving the formation of some stable **PTAA**$^{+\cdot}$ species. This could translate to a considerable improvement in PCE for both **P1** and **PTAA**$_{LMw}$, from undoped to doped.

On the other hand, the UV-Vis spectra of **P3** confirms the inertness of the latter toward doping; indeed, the lack of any additional peak at 500 nm indicates that the polymer is not able to form stable **P3**$^{+\cdot}$ species. Considering the structural similarity between **P3** and **PTAA**, the peculiar behavior of the former could be related to the presence of the additional PTZ unit that likely jeopardizes the stability of radical cation generation. This is ascribable to the non-planar "butterfly" configuration of PTZ that, if coupled with highly substituted backbones (i.e., two methyl groups at the *ortho* position, which distort the sp^3 nature of triphenylamine), causes a loss of conjugation and hinders the intrachain transfer mechanism.[67,74] The UV response of doped **P2** (See Figure S25, Supporting Information) presents a slight bump at $\approx$ 550 nm, as already reported in the literature for doped double-substituted TPA systems.[72] This peak is significantly less intense compared to **P1**, due to a probable destabilization of radical cations upon oxidation, related to an increased steric hindrance. Although **P2** is able to generate **P2**$^{+\cdot}$ and hence increase its conductivity, the shortening in CCL could partially counterbalance this: indeed, smaller polymeric grains would increase the number of grain boundaries, leading to more likely recombination reactions, limiting the PCE of the final devices.[75] The peculiarity of **P4** can also be resolved via the UV absorbance spectra of the doped film, which has a similar shape to that of the undoped state but with an increased intensity of peaks at $\approx$ 380 and $\approx$ 500 nm (See Figure S25, Supporting Information), supporting the generation of stable **P4**$^{+\cdot}$ species at both the PTZ or the TPA site. This effect is caused by the D-A nature of the polymer, as the increase in doping induces additional electrostatic interaction between polymer chains.

To further validate the hypothesis originating from spectroscopic and structural analyses, we fabricated F-PSC based on doped HTMs. Devices were fabricated using Li TFSI, and tBP doped **P1-4** and **PTAA**$_{HMw/LMw}$ using both toluene and THF.

In agreement with the previous reported data, **P1** demonstrated the best efficiency improvement after doping with a champion PCE of 9.06%, outperforming **PTAA**$_{LMw}$ in THF (PCE 8.25%) and comparable to **PTAA**$_{HMw/LMw}$ in toluene (Champion PCE$_{HMw}$ 11.89% / Champion PCE$_{LMw}$ 9.34%) (**Figure 5b**). It should be noted that the standard doping conditions used for **P1-4** are those pre-optimized for **PTAA**, leaving room for device performance improvement for the novel **P1-4** HTMs. The boost in **P1** performance is mainly ascribable to the higher J_{sc}, as a consequence of the more efficient charge extraction induced (Figure 5d). In fact, for **P1-4** the performance improvement is mainly determined by the J_{SC} behavior: for all polymers, the current densities in undoped devices are < 2 mA cm^{-2}, but, upon

**ADVANCED
SCIENCE NEWS**
www.advancedsciencenews.com

**ADVANCED
SUSTAINABLE
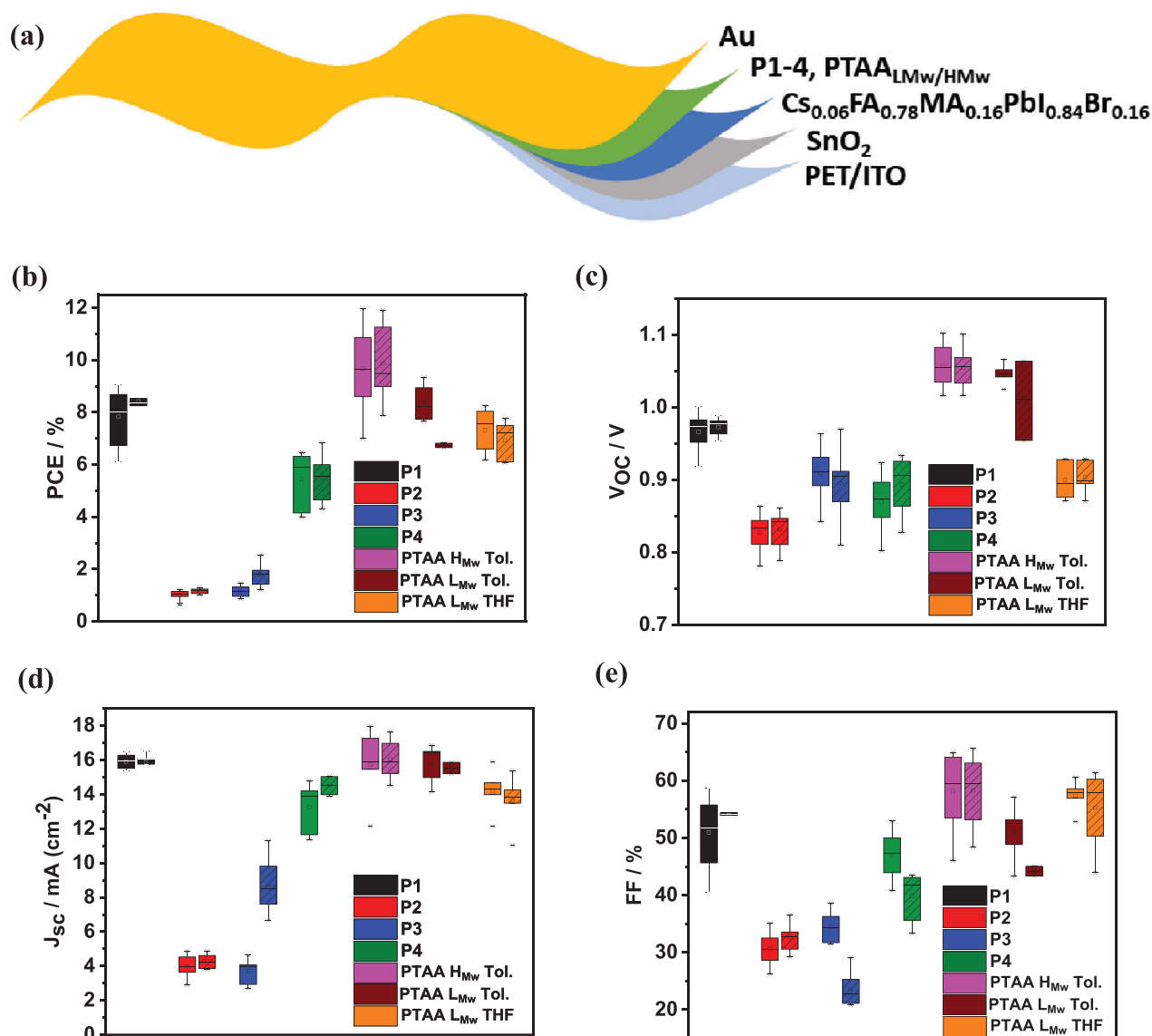SYSTEMS**
www.advsustainsys.com

Figure 5. a) Schematic design of flexible n-i-p devices produced. Box Plot of Photovoltaic parameters b) PCE c) V_{oc} d) J_{sc} e) FF from doped devices of **P1-4** and **PTAA**. Dashed boxes indicate REV scan.

doping, **P1** and **P4** reach $J_{SC} > 12$ mA cm^{-2} (average PCE of ≈8% and ≈6%, respectively), while **P2** and **P3** only reach average values of 4 and 8 mA/cm^2 respectively (≈1% PCE, no significant change from the undoped HTMs), confirming the GWAXS predictions of inefficient generation of radical cations in both **P2** and **P3**. This trend also reflects the observation that upon doping, the repetition units of **P1** and **P4** increase significantly, whereas they remain largely unchanged for **P2** and **P3**, suggesting that the packing of the material dramatically affects the charge extraction capabilities of the device. Similarly, while the Fill-Factor (FF) for **P1-4** starts from values around 25% in the undoped devices, only **P1** and **P4** increase that value to ≈ 50% and ≈ 40% respectively after doping, again suggesting resistive or charge transport limitations in the doped **P2** and **P3**. On the other hand, the higher crystallinity upon doping observed by GWAXS could explain the slight increase in both V_{OC} and FF due to the lower amount of

recombination sites and more favored interactions between polymer crystallites (Figure 5c,e), however V_{OC} values for **P1-4** devices are still consistently lower than those of PTAA in toluene, suggesting the presence of non-radiative recombination losses induced by non-ideal interface between the novel HTMs and the active layer. By observing the differences between **PTAA$_{LMw}$** in toluene and THF, it is evident that the solvent impacts the efficiency of the device, with the most notable effect on the V_{OC}. It is well documented in the literature that V_{OC} losses mainly derive from interfacial recombination events.[76] In spin-coating depositions, the solvent is one of the parameters that affect film morphology;[77] as such, switching from toluene to THF could jeopardize the formation of a smooth HTM/PSK interface. As such, we decided to evaluate the PSK wettability via contact angle analysis of both THF and toluene. Indeed, both the solvents allow a proper wettability of 3C-Perovskite film (CA < 10°, see
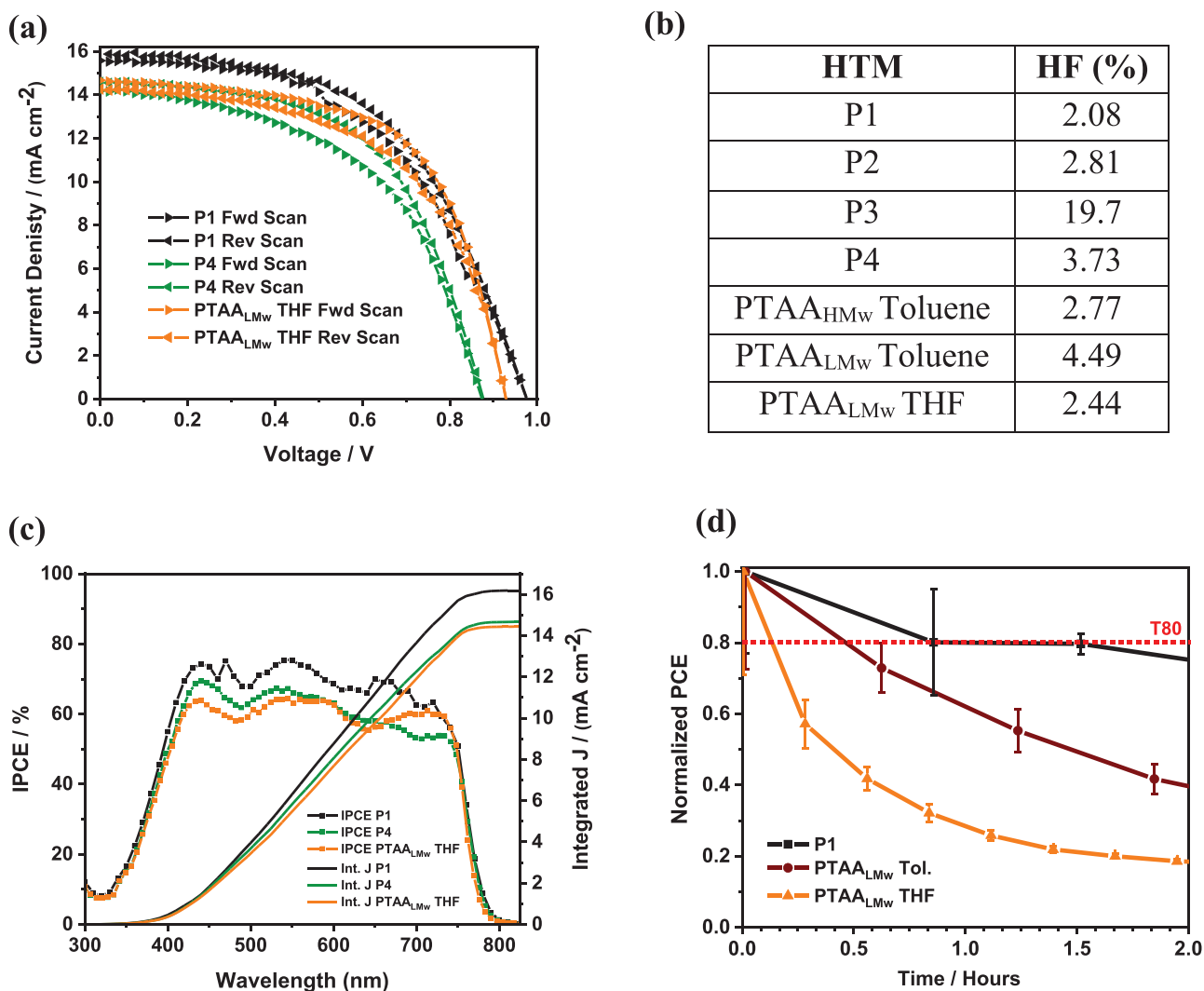
(a)

(b)

HTM	HF (%)
P1	2.08
P2	2.81
P3	19.7
P4	3.73
$PTAA_{HMw}$ Toluene	2.77
$PTAA_{LMw}$ Toluene	4.49
$PTAA_{LMw}$ THF	2.44

(c)

(d)

Figure 6. a) J-V Curves of **P1**, **P4**, $PTAA_{LMw}$ in THF b) Table showing Hysteresis Factor (HF) for **P1-4** and $PTAA_{HMw}$ and $PTAA_{LMw}$ in toluene and THF c) IPCE and integrated current density of **P1**, **P4**, $PTAA_{LMw}$ in THF d) Light Soaking experiment of unencapsulated doped devices of **P1**, $PTAA_{LMw}$ in THF and toluene, all performed in ambient air conditions.

Figure S26, Supporting Information). Since the wettability seems not to play a key role, the lower performance of THF-processed devices could be likely ascribed to the limited solubility of **PTAA**. Additionally, the same argument can be extended to the V_{OC} values experienced by **P1-4** devices, that are consistently lower than those of $PTAA_{HMw/LMw}$ in toluene. Indeed, this most likely suggests the presence of non-radiative recombination losses induced by non-ideal interfaces of the synthesized polymers with the 3C-Perovskite.[76b,78]

The difference between $PTAA_{HMw}$ and $PTAA_{LMw}$ is as expected because larger molecular weights improve the efficiency of the device by providing slower recombination dynamics at the interface, derived by prolonged stability of the charges.[57b] Despite having a difference of 80 kDa in M_W, **P1** and $PTAA_{HMw}$ displayed similar PCEs. This is of particular interest due to two main reasons: (i) a smaller Mw increases the processability of the polymeric HTMs at wider ranges of concentrations and expands the window of solvent processability, paving the way toward non-

toxic, -aromatic and -halogenated solvents, while (ii) smaller Mw systems are synthetically simpler and usually employ more sustainable reaction conditions.[57b]

By examining the JV curves of the best performing devices (**Figure 6**a) it was also decided to calculate the hysteresis factor (HF)[79] (Figure 6b). Hysteresis in solar cells is a phenomenon that yields different JV curves depending on different scan directions. This is primarily derived from the response of mobile ionic charges to external biases, causing them to move and accumulate at the various interfaces, leading to recombination events and impediments on charge extraction.[80] All polymers show similar HFs except **P3**, most likely deriving from poor interfacial interactions that deteriorate the hysteresis. IPCE measurements (See Figure S27, Supporting Information) revealed that **P1** and **P4** are more efficient in converting incident photons to electrons than $PTAA_{LMw}$ in THF, and confirmed the photocurrent produced from the J-V curves. It can also be noted that **P1** does not heavily change the spectral response IPCE (Figure 6c)

**ADVANCED
SCIENCE NEWS**

www.advancedsciencenews.com

**ADVANCED
SUSTAINABLE
SYSTEMS**

www.advsustainsys.com

of the solar cell toward incident light with respect to $PTAA_{LMw}$ in or THF, as expected from similar photophysical properties. (Figure 1a,b) On the other hand, **P4** sees a slight dip in IPCE (Figure 6c) with respect to $PTAA_{LMw}$ at 650–750 nm which can be correlated to the emission profile of **P4** (Figure 1b) in the same region, which most likely influences the hole extraction mechanism.

After the initial screening, unencapsulated devices based on the most promising polymer (i.e., **P1**) were tested for operational stability under continuous 1 Sun illumination in air at room temperature (≈ 25 °C) and ambient humidity ($\approx 30\%$ RH) by tracking the maximum power point (MPP). The operational stability of $PTAA_{LMw}$ in toluene and THF unencapsulated devices are also tracked (Figure 6d). All the analyzed devices experienced an initial, quite fast but somehow expected from previous experience,[16] burn-in process most likely associated with the photodegradation of PbI_2 precursor into metallic lead,[81] with the efficiency dropping significantly within the first 5 h. $PTAA_{LMw}$ **THF**, $PTAA_{LMw}$ **Toluene,** and **P1** had T80 (i.e., the time at which the device reaches 80% of its initial PCE) of ≈ 8, ≈ 29, and ≈ 53 mins, respectively, with P1 outperforming both $PTAA_{LMw}$ **THF** (+ 400%) and $PTAA_{LMw}$ **Toluene** (+80%). Afterwards, while $PTAA_{LMw}$ **Toluene** and $PTAA_{LMw}$ **THF** experienced an exponential decay of performance, achieving 20% after ≈ 5 and ≈ 2 h of ageing, respectively, **P1** displays a less severe degradation, with a halving of the PCE after 20 hours (compared to ≈ 1.5 h or ≈ 0.5 h required for $PTAA_{LMw}$ **Toluene** and $PTAA_{LMw}$ **THF**, respectively). Examining thoroughly the photovoltaic parameters determining the PCE, the V_{OC} remains almost constant throughout the ageing period for all devices, whereas the J_{SC} values evolution replicates the PCE's trend (See Figure S28, Supporting Information). A possible explanation of this could rely on the presence of the PTZ scaffold in **P1**: indeed, in unencapsulated devices, oxygen plays a key role in the accelerated photodegradation of perovskites due to the formation of the highly reactive superoxide (O_2^-) originating from the photogenerated radical.[82] PTZ are well known for showing radical scavenging properties,[83] which could hamper the formation of the superoxide, slowing down the degradation of the active layer. It can also be observed a faster degradation rate for **PTAA** deposited with **THF** rather than **Toluene**. This could result from the poorer solubility of **PTAA** in THF, which results in an inefficient coverage of the perovskite layer leading to a more severe permeation of both oxygen and moisture.

3. Conclusions

In this work, we propose four novel PTAA-based polymers (coded **P1-4**) as HTMs in n-i-p F-PSCs. The polymers were designed aiming to be processed with environmentally harmless solvents (THF) to replace the aromatic and/or halogenated ones conventionally used (toluene/chlorobenzene). To ensure a proper solubility in greener solvents, triarylamine moieties (differing for the number of methyl pendants) were functionalized with a phenothiazine core (**P1-3**) or with an additional benzothiadiazole unit (**P4**). Interestingly, the structural modifications allow us to gain insightful information on both the crystallinity and the polymeric arrangement in the solid state, which dramatically impact the photoelectrochemical features of the resulting F-PSC. Among the polymers, **P2-4** displayed limited to modest device

power conversion efficiencies (Champion PCE's **P2** = 1.21%, **P3** = 1.47%, **P4** = 6.47%). On the other hand, **P1** was found to be the best-performing one (Champion PCE = 9.06% if processed from THF solution), mainly due to an efficient polymer chain-packing (as proved by GWAXS analysis) and a favorable vertical charge transfer. **P1** outperformed the state-of-the-art reference **PTAA** with comparable molecular weight, when the latter is processed in THF and equalized the PCE of toluene processed one (PCE $PTAA_{LMw}$ in THF = 8.25%, $PTAA_{LMw}$ in toluene = 9.34%). These results are very promising considering that **P1** device performance could be further improved by the optimization of dopants that are, in turns, specific for **PTAA** only. Although **PTAA** with a high molecular weight led to better performances (Champion PCE = 11.89% if processed from toluene solution), it suffered from a more severe degradation than **P1** under light soaking measurements, whose stability is ascribable to the presence of the PTZ scaffold. Overall, we presented a thoughtfully designed series of polymers showing comparable PCE values with respect to the state-of-the-art **PTAA,** but allowing a greener and safer device processing. The promising and competitive efficiencies of PSCs embedding **P1** as HTM have allowed for the establishment of a definition of a new class of PTAA-derived polymers, specifically designed to be synthesized and deposited with more sustainable strategies, which showed improved operational and storage stability, crucial parameters for the commercialization of PSCs. Albeit, the preservation of the overall efficiency (or even the better performance with respect to PTAA processed in THF) by improving the greenness of the HTM is a remarkable results per se, further optimization is actually ongoing focusing (i) on the nature and concentration of the dopants and (ii) on polymer engineering to make HTMs compatible with even greener solvents, widening the implementation to different device architectures (e.g., p-i-n) and high performing glass-based devices. We are fairly convinced that this study will serve as a cornerstone to change the direction of the optimization of materials for PSCs from an efficiency-driven concept to a perspective in which the latter is coupled with the proposition of green-inspired processes and green-compatible materials toward truly for sustainable fabrication of PSC's.

4. Experimental Section

Materials: N,N-Bis(4-bromophenyl)-2,4,6-trimethylaniline and Tetrakis(triphenylphosphine) palladium(0) were purchased from TCI Chemicals and used as received. Palladium(II) acetate, RuPhos, *p*-Bromotoluene, 4-Bromo-*m*-xylene, and Diphenylamine were purchased from Sigma-Aldrich and used as received. N-Bromosuccinimide, 4,7-Dibromo-2,1,3-benzothiadiazole, and Aliquat 336 were purchased from ABCR and used as received. Potassium carbonate was purchased from Fluka Chemicals and used as received. Solvents toluene, tetrahydrofuran, and chloroform were all ACS reagent grade purchased from Sigma-Aldrich and used as received.

Tin (IV) oxide (SnO_2) colloidal dispersion in H_2O (15 wt.%) was purchased from Alfa Aesar; formamidinium iodide (FAI) and methylammonium bromide (MABr) was purchased for Greatcell Solar; lead iodide (PbI_2), lead bromide ($PbBr_2$) and caesium iodide (CsI) were purchased from TCI chemicals; bis(trifluoromethylsulfonyl)imide lithium salt (Li TFSI) and 4-tert-butylpyridine (tBP) were purchased from Sigma-Aldrich; PTAA at different molecular weights were purchased from Solaris Chem; the solvents N,N-dimethylformamide (DMF), dimethyl sulfoxide (DMSO)

**ADVANCED
SCIENCE NEWS**

www.advancedsciencenews.com

**ADVANCED
SUSTAINABLE
SYSTEMS**

www.advsustainsys.com

chlorobenzene (CB) and acetonitrile (ACN) were all anhydrous and purchased from Sigma-Aldrich.

Materials Characterization: ^{1}H NMR and ^{13}C NMR spectra were acquired by a JEOL JNM-ECZR 600 MHz NMR Spectrometer, using CDCl$_3$ or THF-d$_8$ as the solvent. UV/Vis spectra in solution were acquired on a UV-1900i double-beam UV-Vis Spectrophotometer using Shimadzu's original LO-RAY-LIGH™ diffraction grating technology, from 800 to 200 nm spectral range. Solid state UV/Vis spectra were acquired on Agilent Cary 5000 Bio spectrophotometer, from 800 to 300 nm, with a scan rate speed of 5 nm s^{-1}. Fluorescence spectra were acquired on a Fluorolog TCSPC Horiba Jobin Yvon Spectrofluorometer, with Xenon lamp and slits varying from 1–15 nm. Thermogravimetric Analysis was performed on a Q600 SDT from TA Instruments with a ramp of 10 °C min^{-1} from 60 to 800 °C in air atmospheres. Differential Scanning Calorimetry experiments were performed on a Q200 DSC from TA Instruments with a ramp of 30 °C min^{-1} to 250 °C and 10 °C min^{-1} to 30 °C, with N$_2$ atmosphere. Cyclic Voltammetry (CV) measurements were performed on an SP-300 BIOLOGIC potentiostat using dichloromethane as the solvent, tetrabutylammonium hexafluorophosphate (TBAPF$_6$) as the supporting electrolyte, Working Electrode (WE) – Carbon black, Counter Electrode (CE) – Pt wire, Reference Electrode (RE) – Ag$^+$/Ag redox couple. Ferrocene was used as internal standard (E$_{red}$ (Fc$^+$/Fc) = 0.7 V vs NHE) Gel Permeation Chromatographic (GPC) analysis was carried out with a Malvern Viscotek system, a Triple Detector, and Polymers **P1-4** were analyzed with a set of two columns Phenogel Phenomenex 100–103 Å (300×4.6 mm, 5μm); THF (HPLC grade, stabilized with BHT, 250 ppm) was used as a carrier solvent (flow rate: 0.35 mL min^{-1}, 30 °C) and an advanced calibration was performed with a narrow polymethyl methacrylate standard. All sample solutions for GPC measurements were prepared at room temperature and then filtered on 0.45 μm PTFE filters. High Resolution Mass Spectrometry (HRMS) was conducted on an *Orbitrap Fusion* mass spectrometer using 4000 V of ion spray voltage, sheath gas of 5 a.u., Ion transfer temperature at 300 °C, vaporizer temperature of 60 °C, with a flow of 10 mL min^{-1} and 50K resolution. Contact Angles were performed on a Theta Lite Attension Optical Tensiometer from Biolin Scientific. A 4 μL drop was deposited using the instrument's dispenser, and both the left-handed and the right-handed angles were continuously analyzed for at least 3 min. The averaged stabilized contact angle after 3 min was taken, and the drop shape was calculated via the Young-Laplace method. A Panalytical Empyrean X-ray diffractometer was used to perform standard diffraction measurements (XRD) in Bragg-Brentano configuration. Detection was accomplished by means of a PixCel 3D detector working in linear mode and a Cu-anode X-ray tube was used as source. Incident optical pathway was set by divergent slits (Size [°] = 0.2177) and patterns were collected in the 5< θ <70° angular range (Step Size [°2θ] = 0.0130, Scan Step Time [s] = 2400). Samples were located onto a flat sample holder for thin films and generator parameters were kept fixed at 45 mA and 40 kV. Grazing incidence Wide Angle X-ray Scattering (GWAXS) measurements were performed to gain information regarding the almost amorphous nature of the polymeric films. Generator parameters were set as previously reported while incident slits were kept 1/32°-1/16°. Brag Brentano configuration was kept with a 2.5° tilt between incident and reflected angle.

Device Fabrication: Flexible PET/ITO substrates, sized 2.5×2.5 cm^2, were laser scribed to obtain 4 electrically isolated areas on the same substrate. They were washed with DI water and Hellmanex detergent, rinsed, and re-immersed in DI water to undergo 10 min in an ultrasonic bath, followed by 10 mins immersed in isopropanol in an ultrasonic bath, and once again 10 mins immersed in DI water in an ultrasonic bath. After 15 min under a UV lamp and ozone treatment, an aqueous colloidal dispersion of SnO$_2$ (15% in weight) from Alfa Aesar was spin-coated statically onto the substrate at 6000 rpm for 45 s (180 μL). The deposited SnO$_2$ thin films were annealed in air at 100 °C and treated under a UV lamp for 25 min prior to perovskite deposition.

For the perovskite precursor solution, 166 mg of FAI, 547 mg of PbI$_2$, 21.6 mg of MABr, 87.2 mg of PbBr$_2$, and 19.5 mg of CsI were dissolved in a mixed solution of solvent mixture DMF:DMSO (3.17:1 vol) and then let to stir for 12 h at room temperature. The as-prepared precursor solution was then deposited onto PET/ITO/SnO$_2$ via static spin coating: the first

step at 1000 rpm for 10 s (85 μL), followed by the second step at 5000 rpm for 30 s, just 7 s before the end of the spinning process, 150 μL of chlorobenzene was dropped on the substrates. The subsequent perovskite films were annealed at 100 °C for 1 h.

P1-4, as well as PTAA (High and Low M$_w$), were dissolved in THF or toluene at a concentration of 12 mg mL^{-1} using 10.5 μL mL^{-1} of LiTFSI (stock solution 170 mg mL^{-1} in acetonitrile) and 5.6 μL mL^{-1} of 4-*tert*-butylpyridine as additives, for doped experiments. The HTMs were then dynamically spin-coated onto the perovskite surface at 1500 rpm for 30 s.

Finally, the cells were completed by thermal evaporation of Au (100 nm) as the top electrode. The devices were masked with an aperture of 0.09 cm^2 to define the active working area.

Device Characterization: The photovoltaic characteristics of flexible devices were measured under standard test conditions (STC, AM1.5 G, 100 mW cm^{-2}, 25 °C) using a Keithley 2420 source meter and an ABET sun 2000 solar simulator. Cells were measured in air (20–22 °C and ±50% RH) without encapsulation and masked with a black tape with 0.09 cm^2 aperture during the measurements. Current Density–Voltage (J–V) curves were recorded at a scan rate of 33 mV s^{-1} in both forward (V = 0 V to V$_{OC}$) and reverse (V$_{OC}$ to V = 0 V) sweeps. The four cells on each substrate were measured simultaneously during the J–V and maximum power point tracking (MPPT). EQE was carried out with a modular testing platform (Arkeo – Cicciresearch s.r.l.) consisting of a white light emitting diode array (4200 K) tuneable up to 200 mW cm^{-2} of optical power density and a high-speed source meter unit. Light Soaking Experiment was performed under the illumination MPPT tracking system composed of a white LED array (4200 K).

Supporting Information

Supporting Information is available from the Wiley Online Library or from the author.

Acknowledgements

Conflict of Interest

The authors declare no conflict of interest.

Author Contributions

D.A.M.A. performed conceptualization, data curation, formal analysis, investigation, methodology, and writing – original draft. G.K. performed data curation, formal analysis, investigation. F.d.R. performed conceptualization, data curation, formal analysis, investigation, project administration.

Data Availability Statement

The data that support the findings of this study are available from the corresponding author upon reasonable request.

Keywords

[1] a) A. Fakharuddin, M. Vasilopoulou, A. Soultati, M. I. Haider, J. Briscoe, V. Fotopoulos, D. Di Girolamo, D. Davazoglou, A. Chroneos, A. R. b. M. Yusoff, A. Abate, L. Schmidt-Mende, M. K. Nazeeruddin, *Sol. RRL* **2020**, *5*, 2000555; b) G. E. Eperon, S. D. Stranks, C. Menelaou, M. B. Johnston, L. M. Herz, H. J. Snaith, *Energy Environ. Sci.* **2014**, *7*, 982; c) S. De Wolf, J. Holovsky, S. J. Moon, P. Loper, B. Niesen, M. Ledinsky, F. J. Haug, J. H. Yum, C. Ballif, *J. Phys. Chem. Lett.* **2014**, *5*, 1035; d) L. M. Herz, *ACS Energy Lett.* **2017**, *2*, 1539; e) S. D. Stranks, G. E. Eperon, G. Grancini, C. Menelaou, M. J. Alcocer, T. Leijtens, L. M. Herz, A. Petrozza, H. J. Snaith, *Science* **2013**, *342*, 341; f) L. Calio, S. Kazim, M. Gratzel, S. Ahmad, *Angew. Chem. Int. Ed.* **2016**, *55*, 14522.

[2] a) Y. Xiong, Z. Yi, W. Zhang, Y. Huang, Z. Zhang, Q. Jiang, X. R. Ng, G. Shen, Y. Luo, X. Li, J. Yang, *Mater. Today Electron.* **2024**, *7*, 100086; b) Z. Yi, X. Li, Y. Xiong, G. Shen, W. Zhang, Y. Huang, Q. Jiang, X. R. Ng, Y. Luo, J. Zheng, W. L. Leong, F. Fu, T. Bu, J. Yang, *Interdiscip. Mater.* **2024**, *3*, 203.

[3] H. Chen, C. Liu, J. Xu, A. Maxwell, W. Zhou, Y. Yang, Q. Zhou, A. S. R. Bati, H. Wan, Z. Wang, L. Zeng, J. Wang, P. Serles, Y. Liu, S. Teale, Y. Liu, M. I. Saidaminov, M. Li, N. Rolston, S. Hoogland, T. Filleter, M. G. Kanatzidis, B. Chen, Z. Ning, E. H. Sargent, *Science* **2024**, *384*, 189.

[4] S. Mishra, S. Ghosh, T. Singh, *ChemSusChem* **2021**, *14*, 512.

[5] M. H. Kumar, N. Yantara, S. Dharani, M. Graetzel, S. Mhaisalkar, P. P. Boix, N. Mathews, *Chem. Commun.* **2013**, *49*, 11089.

[6] N. Ren, L. Tan, M. Li, J. Zhou, Y. Ye, B. Jiao, L. Ding, C. Yi, *iEnergy* **2024**, *3*, 39.

[7] a) S. K. Podapangi, F. Jafarzadeh, S. Mattiello, T. B. Korukonda, A. Singh, L. Beverina, T. M. Brown, *RSC Adv.* **2023**, *13*, 18165; b) Y. Ma, Z. Lu, X. Su, G. Zou, Q. Zhao, *Adv. Energy Sustainability Res.* **2022**, *4*, 2200133.

[8] M. M. H. Desoky, M. Bonomo, R. Buscaino, A. Fin, G. Viscardi, C. Barolo, P. Quagliotto, *Energies* **2021**, *14*, 2279.

[9] R. Singh, P. K. Singh, B. Bhattacharya, H.-W. Rhee, *App. Mat. Today* **2019**, *14*, 175.

[10] D. Di Girolamo, F. Di Giacomo, F. Matteocci, A. G. Marrani, D. Dini, A. Abate, *Chem. Sci.* **2020**, *11*, 7746.

[11] B. Wang, S. Nam, S. Limbu, J. S. Kim, M. Riede, D. D. C. Bradley, *Adv. Electron. Mater.* **2022**, *8*, 2101253.

[12] L. Chen, Q. Xie, L. Wan, W. Zhang, S. Fu, H. Zhang, X. Ling, J. Yuan, L. Miao, C. Shen, X. Li, W. Zhang, B. Zhu, H.-Q. Wang, *ACS Appl. Energy Mater* **2019**, *2*, 5862.

[13] M. Shahinuzzaman, S. Afroz, H. Mohafez, M. S. Jamal, M. U. Khandaker, A. Sulieman, N. Tamam, M. A. Islam, *Nanomaterials* **2022**, *12*, 3003.

[14] X. Yin, Z. Song, Z. Li, W. Tang, *Energy Environ. Sci.* **2020**, *13*, 4057.

[15] F. M. Rombach, S. A. Haque, T. J. Macdonald, *Energy Environ. Sci.* **2021**, *14*, 5161.

[16] F. De Rossi, G. Renno, B. Taheri, N. Yaghoobi Nia, V. Ilieva, A. Fin, A. Di Carlo, M. Bonomo, C. Barolo, F. Brunetti, *J. Power Sources* **2021**, *494*, 229735.

[17] X. Fan, W. Nie, H. Tsai, N. Wang, H. Huang, Y. Cheng, R. Wen, L. Ma, F. Yan, Y. Xia, *Adv. Sci.* **2019**, *6*, 1900813.

[18] W. S. Yang, B. W. Park, E. H. Jung, N. J. Jeon, Y. C. Kim, D. U. Lee, S. S. Shin, J. Seo, E. K. Kim, J. H. Noh, S. I. Seok, *Science* **2017**, *356*, 1376.

[19] a) J. H. Noh, S. H. Im, J. H. Heo, T. N. Mandal, S. I. Seok, *Nano Lett* **2013**, *13*, 1764; b) J. H. Heo, S. H. Im, J. H. Noh, T. N. Mandal, C.-S. Lim, J. A. Chang, Y. H. Lee, H.-j. Kim, A. Sarkar, M. K. Nazeeruddin, M. Grätzel, S. I. Seok, *Nat. Photonics* **2013**, *7*, 486.

[20] Y. Ko, Y. Kim, C. Lee, Y. Kim, Y. Jun, *ACS Appl. Mater. Interfaces* **2018**, *10*, 11633.

[21] M. Zhang, D. Xin, X. Zheng, Q. Chen, W.-H. Zhang, *ACS Sustainable Chem. Eng.* **2020**, *8*, 13126.

[22] J. Gong, S. B. Darling, F. You, *Energy Environ. Sci.* **2015**, *8*, 1953.

[23] R. Søndergaard, M. Hösel, D. Angmo, T. T. Larsen-Olsen, F. C. Krebs, *Mater. Today* **2012**, *15*, 36.

[24] B. Yang, M. Zhang, G. Qiao, H. Zhang, *Sol. RRL* **2023**, *7*, 2300217.

[25] A. Roy, A. Ghosh, S. Bhandari, S. Sundaram, T. K. Mallick, *Buildings* **2020**, *10*, 129.

[26] a) X. Yu, D. Gao, Z. Li, X. Sun, B. Li, Z. Zhu, Z. Li, *Angew. Chem. Int. Ed.* **2023**, *62*, e202218752; b) Y. Li, K. R. Scheel, R. G. Clevenger, W. Shou, H. Pan, K. V. Kilway, Z. Peng, *Advanced Energy Materials* **2018**, *8*, 1801248; c) G. You, L. Li, S. Wang, J. Cao, L. Yao, W. Cai, Z. Zhou, K. Li, Z. Lin, H. Zhen, Q. Ling, *Adv. Energy Mater. 2021 12*, 2102697; d) P. Yan, D. Yang, H. Wang, S. Yang, Z. Ge, *Energy Environ. Sci.* **2022**, *15*, 3630.

[27] Y.-J. A. Hui-Seon Kim, J. I. Kwak, H. J. Kim, H. S. Jung, N.-G. Park, *ACS Energy Lett* **2022**, *7*, 1154.

[28] J. Lee, G. W. Kim, M. Kim, S. A. Park, T. Park, *Adv. Energy Mater.* **2020**, *10*, 1902662.

[29] M. Mahboubi, N. Kazempour, *Songklanakarin J. Sci. Technol.* **2014**, *36*, 83.

[30] *EFSA J.* **2008**, *6*, 855.

[31] a) R. Vidal, J.-A. Alberola-Borràs, S. N. Habisreutinger, J.-L. Gimeno-Molina, D. T. Moore, T. H. Schloemer, I. Mora-Seró, J. J. Berry, J. M. Luther, *Nat. Sustain.* **2020**, *4*, 277; b) H. Lu, B. He, Y. Ji, Y. Shan, C. Zhong, J. Xu, J. LiuYang, F. Wu, L. Zhu, *Chem. Eng. J.* **2020**, *385*, 123976; c) M. Tobiszewski, J. Namieśnik, F. Pena-Pereira, *Green Chem.* **2017**, *19*, 1034.

[32] a) V. Pace, P. Hoyos, L. Castoldi, P. Dominguez de Maria, A. R. Alcantara, *ChemSusChem* **2012**, *5*, 1369; b) S. Monticelli, L. Castoldi, I. Murgia, R. Senatore, E. Mazzeo, J. Wackerlig, E. Urban, T. Langer, V. Pace, *Monatsh. Chem.* **2017**, *148*, 37.

[33] K. Jiang, F. Wu, G. Zhang, L. Zhu, H. Yan, *Sol. RRL* **2019**, *3*, 1900061.

[34] a) G. Wu, Y. Zhang, R. Kaneko, Y. Kojima, K. Sugawa, A. Islam, J. Otsuki, S. Liu, *Synth. Met.* **2020**, *261*, 116323; b) A. Farokhi, H. Shahroosvand, G. D. Monache, M. Pilkington, M. K. Nazeeruddin, *Chem. Soc. Rev* **2022**, *51*, 5974.

[35] a) J. Salunke, X. Guo, Z. Lin, J. R. Vale, N. R. Candeias, M. Nyman, S. Dahlström, R. Österbacka, A. Priimagi, J. Chang, P. Vivo, *ACS Appl. Energy Mater.* **2019**, *2*, 3021; b) F. Zhang, S. Wang, H. Zhu, X. Liu, H. Liu, X. Li, Y. Xiao, S. M. Zakeeruddin, M. Grätzel, *ACS Energy Lett* **2018**, *3*, 1145.

[36] H. Fu, Y. Li, J. Yu, Z. Wu, Q. Fan, F. Lin, H. Y. Woo, F. Gao, Z. Zhu, A. K. Jen, *J. Am. Chem. Soc.* **2021**, *143*, 2665.

[37] a) C. Bi, B. Chen, H. Wei, S. DeLuca, J. Huang, *Adv. Mater.* **2017**, *29*, 1605900; b) M. M. Tavakoli, R. Tavakoli, *Phys. Status Solidi RRL* **2020**, *15*, 2000147; c) Z. Wang, Y. Lu, Z. Xu, J. Hu, Y. Chen, C. Zhang, Y. Wang, F. Guo, Y. Mai, *Adv. Sci.* **2021**, *8*, e2101856; d) S. Wu, Z. Li, J. Zhang, X. Wu, X. Deng, Y. Liu, J. Zhou, C. Zhi, X. Yu, W. C. H. Choy, Z. Zhu, A. K. Jen, *Adv. Mater.* **2021**, *33*, 2105539; e) Y. Wang, L. Duan, M. Zhang, Z. Hameiri, X. Liu, Y. Bai, X. Hao, *Sol. RRL* **2022**, *6*, 2200234.

[38] I. Maluenda, O. Navarro, *Molecules* **2015**, *20*, 7528.

[39] M. M. H. Desoky, F. Cruciani, P. Quagliotto, G. Viscardi, *J. Mol. Struct.* **2024**, *1304*, 137635.

[40] I. Ando, *Polym. J.* **2012**, *44*, 734.

[41] a) G. Wang, Y. Wu, W. Ding, G. Yu, Z. Hu, H. Wang, S. Liu, Y. Zou, C. Pan, *J. Mater. Chem. A* **2015**, *3*, 14217; b) J. Chen, J. Xia, W. J. Gao, H. J. Yu, J. X. Zhong, C. Jia, Y. S. Qin, Z. She, D. B. Kuang, G. Shao, *ACS Appl. Mater. Interfaces* **2020**, *12*, 21088.

[42] J. M. Marin-Beloqui, S. Gómez, H. I. Gonev, M. Comí, M. Al-Hashimi, T. M. Clarke, *Chem. Sci.* **2023**, *14*, 812.

[43] M. H. Tahir, T. Mubashir, T. U. H. Shah, A. Mahmood, *J. Phys. Org. Chem.* **2018**, *32*, e3909.

[44] W. Wu, J. Yang, J. Hua, J. Tang, L. Zhang, Y. Long, H. Tian, *J. Mater. Chem.* **2010**, *20*, 1772.

[45] a) Y.-C. Huang, T.-C. Lu, C.-I. Huang, *Polymer* **2013**, *54*, 6489; b) R. Noriega, A. Salleo, A. J. Spakowitz, *Proc. Natl. Acad. Sci. USA* **2013**, *110*, 16315.

[46] L. Ning, G. Han, Y. Yi, *J. Mater. Chem. C* **2019**, *7*, 14198.

[47] a) J. Liao, P. Zheng, G. Xu, F. Weng, L. Zeng, Z. Huang, Y. Chen, Y. Yang, J. Chen, Z. Qiu, H. Zhao, Y. Xu, *Dyes Pigm* **2022**, *197*, 109834; b) T. Zhong, C. Xiao, B. Xiao, L. Hu, Z. Li, F. Guo, X. Wang, M. Zhang, S. Lei, R. Yang, *Polym. Chem.* **2022**, *13*, 4944.

[48] J. C. S. Costa, R. J. S. Taveira, C. F. R. A. C. Lima, A. Mendes, L. M. N. B. F. Santos, *Opt. Mater.* **2016**, *58*, 51.

[49] Z.-Z. Sun, Y.-L. Xu, W.-L. Ding, W.-J. Chi, *Synth. Met.* **2019**, *247*, 157.

[50] Y. Xu, Q. Chu, D. Chen, A. Fuentes, *Front. Mech.* **2021**, *7*, 744001.

[51] R. Vaillon, S. Parola, C. Lamnatou, D. Chemisana, *Cell Rep. Phys. Sci.* **2020**, *1*, 100267.

[52] S. Thokala, S. P. Singh, *ACS Omega* **2020**, *5*, 5608.

[53] a) Z. Qian, Z. Cao, L. Galuska, S. Zhang, J. Xu, X. Gu, *Macromol. Chem. Phys.* **2019**, *220*, 1900062; b) C. Mayer, F. Sciortino, C. N. Likos, P. Tartaglia, H. Löwen, E. Zaccarelli, *Macromolecules* **2008**, *42*, 423.

[54] a) T. Malinauskas, D. Tomkute-Luksiene, R. Sens, M. Daskeviciene, R. Send, H. Wonneberger, V. Jankauskas, I. Bruder, V. Getautis, *ACS Appl. Mater. Interfaces* **2015**, *7*, 11107; b) D. Zhang, D. Li, Y. Hu, A. Mei, H. Han, *Commun. Mater.* **2022**, *3*, 58; c) S. Mazumdar, Y. Zhao, X. Zhang, *Front. Electron.* **2021**, *2*, 712785; d) K. Rakstys, C. Igci, M. K. Nazeeruddin, *Chem. Sci.* **2019**, *10*, 6748; e) Z. Li, C. Xiao, Y. Yang, S. P. Harvey, D. H. Kim, J. A. Christians, M. Yang, P. Schulz, S. U. Nanayakkara, C.-S. Jiang, J. M. Luther, J. J. Berry, M. C. Beard, M. M. Al-Jassim, K. Zhu, *Energy Environ. Sci.* **2017**, *10*, 1234.

[55] S. Bobba, S. Carrara, J. Huisman, F. Mathieux, C. Pavel, *Publications Office* **2020**, https://doi.org/10.2873/58081.

[56] P. Huang, Manju, S. K, L. Lezama, R. Misra, S. Ahmad, *ACS Appl. Mater. Interfaces* **2021**, *13*, 33311.

[57] a) I. Lee, N. Rolston, P.-L. Brunner, R. H. Dauskardt, *ACS Appl. Mater. Interfaces* **2019**, *11*, 23757; b) N. Yaghoobi Nia, M. Bonomo, M. Zendehdel, E. Lamanna, M. M. H. Desoky, B. Paci, F. Zurlo, A. Generosi, C. Barolo, G. Viscardi, P. Quagliotto, A. Di Carlo, *ACS Sustainable Chem. Eng.* **2021**, *9*, 5061.

[58] Q. Zhao, R. Wu, Z. Zhang, J. Xiong, Z. He, B. Fan, Z. Dai, B. Yang, X. Xue, P. Cai, S. Zhan, X. Zhang, J. Zhang, *Org. Electron.* **2019**, *71*, 106.

[59] K. T. Nielsen, K. Bechgaard, F. C. Krebs, *Macromolecules* **2005**, *38*, 658.

[60] S. Griggs, A. Marks, D. Meli, G. Rebetez, O. Bardagot, B. D. Paulsen, H. Chen, K. Weaver, M. I. Nugraha, E. A. Schafer, J. Tropp, C. M. Aitchison, T. D. Anthopoulos, N. Banerji, J. Rivnay, I. McCulloch, *Nat. Commun.* **2022**, *13*, 7964.

[61] A. Luzio, L. Criante, V. D'Innocenzo, M. Caironi, *Sci. Rep.* **2013**, *3*, 3425.

[62] a) D. Khim, A. Luzio, G. E. Bonacchini, G. Pace, M. J. Lee, Y. Y. Noh, M. Caironi, *Adv. Mater.* **2018**, *30*, 1705463; b) N.-K. Kim, S.-Y. Jang, G. Pace, M. Caironi, W.-T. Park, D. Khim, J. Kim, D.-Y. Kim, Y.-Y. Noh, *Chem. Mater.* **2015**, *27*, 8345.

[63] H E. Swanson, N T. Gilfrich, G. M. Ugrinic, *Circular of the Bureau of Standards* **1955**, *5*, 34.

[64] F. Xu, Y. Tian, W. Wang, Y. Zhu, L. Zeng, B. Yao, Z. Fang, H. Xu, R. Xu, F. Xu, F. Hong, L. Wang, *J. Mater. Sci.: Mater. Electron.* **2019**, *30*, 8381.

[65] M. Pandey, N. Kumari, S. Nagamatsu, S. S. Pandey, *J. Mater. Chem. C* **2019**, *7*, 13323.

[66] Z. Peng, L. Ye, H. Ade, *Mater. Horiz.* **2022**, *9*, 577.

[67] S. Tsarev, I. K. Yakushchenko, S. Y. Luchkin, P. M. Kuznetsov, R. S. Timerbulatov, N. N. Dremova, L. A. Frolova, K. J. Stevenson, P. A. Troshin, *Sustainable Energy Fuels* **2019**, *3*, 2627.

[68] a) E. Li, C. Liu, H. Lin, X. Xu, S. Liu, S. Zhang, M. Yu, X. M. Cao, Y. Wu, W. H. Zhu, *Adv. Funct. Mater.* **2021**, *31*, 2103847; b) W. Gomulya, G. D. Costanzo, E. J. de Carvalho, S. Z. Bisri, V. Derenskyi, M. Fritsch, N. Frohlich, S. Allard, P. Gordiichuk, A. Herrmann, S. J. Marrink, M. C. dos Santos, U. Scherf, M. A. Loi, *Adv. Mater.* **2013**, *25*, 2948; c) L. Canil, J. Salunke, Q. Wang, M. Liu, H. Köbler, M. Flatken, L. Gregori, D. Meggiolaro, D. Ricciarelli, F. De Angelis, M. Stolterfoht, D. Neher, A. Priimagi, P. Vivo, A. Abate, *Adv. Energy Mater.* **2021**, *11*, 2101553.

[69] a) D. Bi, G. Boschloo, A. Hagfeldt, *Nano* **2014**, *09*, 1440001; b) S. Song, E. Y. Park, B. S. Ma, D. J. Kim, H. H. Park, Y. Y. Kim, S. S. Shin, N. J. Jeon, T. S. Kim, J. Seo, *Adv. Energy Mater.* **2021**, *11*, 2003382.

[70] a) S. C. Creason, J. Wheeler, R. F. Nelson, *J. Org. Chem.* **1972**, *37*, 4440; b) K. Sreenath, C. V. Suneesh, V. K. Kumar, K. R. Gopidas, *J. Org. Chem* **2008**, *73*, 3245; c) O. Yurchenko, D. Freytag, L. zur Borg, R. Zentel, J. Heinze, S. Ludwigs, *J. Phys. Chem. B* **2012**, *116*, 30; d) P. Blanchard, C. Malacrida, C. Cabanetos, J. Roncali, S. Ludwigs, *Polym. Int.* **2018**, *68*, 589.

[71] a) J. A. Christensen, B. T. Phelan, S. Chaudhuri, A. Acharya, V. S. Batista, M. R. Wasielewski, *J. Am. Chem. Soc.* **2018**, *140*, 5290; b) A. A. Golriz, T. Suga, H. Nishide, R. Berger, J. S. Gutmann, *RSC Adv.* **2015**, *5*, 22947; c) I. I. Abu-Abdoun, A. Ledwith, *Eur. Polym. J.* **1997**, *33*, 1671.

[72] Y. Kim, E. H. Jung, G. Kim, D. Kim, B. J. Kim, J. Seo, *Adv. Energy Mater.* **2018**, *8*, 1801668.

[73] K. Yuan Chiu, T. Xiang Su, J. Hong Li, T.-H. Lin, G.-S. Liou, S.-H. Cheng, *J. Electroanal. Chem.* **2005**, *575*, 95.

[74] Y. Liu, Y. Lu, L. Ding, C. K. Pan, Y. C. Xu, T. Y. Wang, J. Y. Wang, J. Pei, *J. Polym. Sci.* **2023**, *61*, 951.

[75] a) T. Heumueller, W. R. Mateker, I. T. Sachs-Quintana, K. Vandewal, J. A. Bartelt, T. M. Burke, T. Ameri, C. J. Brabec, M. D. McGehee, *Energy Environ. Sci.* **2014**, *7*, 2974; b) D. Qian, Z. Zheng, H. Yao, W. Tress, T. R. Hopper, S. Chen, S. Li, J. Liu, S. Chen, J. Zhang, X. K. Liu, B. Gao, L. Ouyang, Y. Jin, G. Pozina, I. A. Buyanova, W. M. Chen, O. Inganas, V. Coropceanu, J. L. Bredas, H. Yan, J. Hou, F. Zhang, A. A. Bakulin, F. Gao, *Nat. Mater.* **2018**, *17*, 703; c) X. K. Chen, M. K. Ravva, H. Li, S. M. Ryno, J. L. Brédas, *Adv. Energy Mater.* **2016**, *6*, 1601325.

[76] a) C. M. Wolff, P. Caprioglio, M. Stolterfoht, D. Neher, *Adv. Mater.* **2019**, *31*, 1902762; b) M. Stolterfoht, P. Caprioglio, C. M. Wolff, J. A. Márquez, J. Nordmann, S. Zhang, D. Rothhardt, U. Hörmann, Y. Amir, A. Redinger, L. Kegelmann, F. Zu, S. Albrecht, N. Koch, T. Kirchartz, M. Saliba, T. Unold, D. Neher, *Energy Environ. Sci.* **2019**, *12*,

**ADVANCED
SCIENCE NEWS**

www.advancedsciencenews.com

**ADVANCED
SUSTAINABLE
SYSTEMS**

www.advsustainsys.com

2778; c) I. Gelmetti, N. F. Montcada, A. Pérez-Rodríguez, E. Barrena, C. Ocal, I. García-Benito, A. Molina-Ontoria, N. Martín, A. Vidal-Ferran, E. Palomares, *Energy Environ. Sci.* **2019**, *12*, 1309.

[77] P.-Y. Chung, M.-H. Cheng, H.-F. Tseng, C.-T. Liu, T.-Y. Chiu, K.-S. Jeng, M.-H. Chi, J.-T. Chen, A. C. S. Appl, *Nano Mater* **2018**, *1*, 2021.

[78] a) A. Ullah, K. H. Park, H. D. Nguyen, Y. Siddique, S. F. A. Shah, H. Tran, S. Park, S. I. Lee, K. K. Lee, C. H. Han, K. Kim, S. Ahn, I. Jeong, Y. S. Park, S. Hong, *Adv. Energy Mater.* **2021**, *12*, 2103175; b) M. Stolterfoht, C. M. Wolff, J. A. Márquez, S. Zhang, C. J. Hages, D. Rothhardt, S. Albrecht, P. L. Burn, P. Meredith, T. Unold, D. Neher, *Nat. Energy* **2018**, *3*, 847; c) M. Stolterfoht, M. Grischek, P. Caprioglio, C. M. Wolff, E. Gutierrez-Partida, F. Peña-Camargo, D. Rothhardt, S. Zhang, M. Raoufi, J. Wolansky, M. Abdi-Jalebi, S. D. Stranks, S. Albrecht, T. Kirchartz, D. Neher, *Adv. Mater.* **2020**, *32*, 2000080.

[79] a) S. N. Habisreutinger, N. K. Noel, H. J. Snaith, *ACS Energy Lett* **2018**, *3*, 2472; b) G. A. Nemnes, C. Besleaga, A. G. Tomulescu, A. Palici, L. Pintilie, A. Manolescu, I. Pintilie, *Solar Energy* **2018**, *173*, 976.

[80] a) D. A. Jacobs, Y. Wu, H. Shen, C. Barugkin, F. J. Beck, T. P. White, K. Weber, K. R. Catchpole, *Phys. Chem. Chem. Phys.* **2017**, *19*, 3094; b) S. van Reenen, M. Kemerink, H. J. Snaith, *J. Phys. Chem. Lett.* **2015**, *6*, 3808; c) C. Li, S. Tscheuschner, F. Paulus, P. E. Hopkinson, J. Kiessling, A. Kohler, Y. Vaynzof, S. Huettner, *Adv. Mater.* **2016**, *28*, 2446.

[81] G. Tumen-Ulzii, C. Qin, D. Klotz, M. R. Leyden, P. Wang, M. Auffray, T. Fujihara, T. Matsushima, J. W. Lee, S. J. Lee, Y. Yang, C. Adachi, *Adv. Mater.* **2020**, *32*, 1905035.

[82] N. Aristidou, I. Sanchez-Molina, T. Chotchuangchutchaval, M. Brown, L. Martinez, T. Rath, S. A. Haque, *Angew. Chem. Int. Ed.* **2015**, *54*, 8208.

[83] M. Dalla Tiezza, T. A. Hamlin, F. M. Bickelhaupt, L. Orian, *ChemMedChem* **2021**, *16*, 3763.